Electronic Supplementary Information for

Constructing Sacrificial Bonds and Hidden Lengths for Ductile Graphene/ Polyurethane Elastomers with Improved Strength and Toughness

Zhongxin Chen, Hongbin Lu*

State Key Laboratory of Molecular Engineering of Polymers, and Department of Macromolecular Science, Fudan University, 220 Handan Road, Shanghai, 200433, China. Tel/Fax: 86-21-5566 4589

*To whom correspondence should be addressed: hongbinlu@fudan.edu.cn.

● This PDF file includes:

1. Instruments
2. Dispersion of HO-GNs in different solvents
3. XPS spectra of GO and HO-GNs
4. Fluorescence study on the non-covalent bonding between pyrenemethanol and graphene
5. XRD and Raman investigation on the structure of graphene
6. SEM fractographs of cryogenically fractured the neat PU and GN/PU elastomer films
7. Dynamic mechanical analysis of the neat PU and composite elastomer films

Figures. S1-S7; References.

● Other Supplementary Materials for this manuscript include the following

1. A video that records the deformation process of HO-GN/PU films.

1. Instruments

1.1 Microscopy investigation

Transmission electron microscopy (TEM) was performed on a JEOL-1230 instrument, operated at 200 kV. The samples for TEM observation were prepared by depositing GO or HO-GNs from the DMF solution (0.1 mg/ml) on holey copper grids.

Atomic force micrographs (AFM) were acquired using a Multimode Nano 4 in the tapping mode. The samples were prepared by depositing the mentioned dispersion on freshly cleaved mica surfaces. The scan rate was 1 Hz, the scan lines were 512 and an ACTA tapping tips (single crystal silicon) was used. The AFM image was directly used without further modification (*e.g.* flattening).

The microstructure of nanocomposite films was observed by using a S-4800 high resolution field emission scanning electron microscopy (FE-SEM). The PU films were fractured in liquid nitrogen. Samples with fracture surfaces on the top were placed on a specimen holder using double-sided carbon conductive tape and then coated with gold.

1.2 FT-IR instrumentation

Fourier transform infrared (FT-IR) spectra were obtained using a NEXUS 670 spectrometer. Each sample was scanned for 64 times with a resolution of 4 cm^{-1}. All the spectra were scanned within the range 400-4000 cm^{-1}.

1.3 XPS-measurements

X-ray photoelectron spectra (XPS) were obtained using a RBD upgraded PHI-5000C ESCA system (Perkin Elmer) with Mg K_α radiation (hν=1253.6 eV). The X-ray gun was operated at 14 kV and 20 mA. Survey spectra (1100-0 eV) were collected using 93.9 eV pass energy, step 1 eV, and an X-ray spot size of 4×10 mm, to obtain the atomic percentage data. High-resolution spectra were collected using 23.5 eV pass energy, step 0.2 eV (0.1 eV for C_{1s} of HO-GNs) and at least 15 scans. The spectral range of interest was collected for C_{1s}, O_{1s} and N_{1s} core-level spectra (300-275, 550-525 and 415-390 eV, respectively). A constant dwell time (100 ms) was used for both survey and high-resolution spectra. The analyzer chamber was degasified and the pressure of the chamber was kept below 10^{-8} torr. All the samples were analyzed at 45^o take off angle, where the effective sampling depth, z, was derived by $z = 3\lambda\cos\theta$ (λ is the effective mean free path for electrons to escape from the surface and its value is roughly 2.5 nm). That is, $\theta = 45^o$, z = 5.3 nm.

To compensate for the surface charging effect, all binding energies (BEs) were corrected according to the C_{1s} hydrocarbon peak at 284.6 eV. The XPS data was fitted using the XPS Peak processing software version 4.1 (Chemistry, CUHK), along with a Shirley background subtraction, a Gaussian sum function, and an iterative least-squares optimization algorithm.[1] Peak positions and boundaries used for deconvolution were determined in terms of the data reported in the literature.[2,3] The full width half maximum (FWHM) of peaks was chosen to be ~2 eV, slightly larger than the literature value,[1-3] which would be reasonable on the basis of the spectrometer condition we used and the tailing of curves. Given the relatively low content of N atoms in GO (0.6%) and HO-GNs (2.2%, mainly from urethane groups), the peak of C-N for C_{1s} core-level spectra was NOT taken into account. In fitting, if three or less subpeaks were used, the C_{1s} core-level spectra have no way to provide rational fitting results. For the N_{1s} core-level spectra, only a broad peak can be fitted and not be divided into subpeaks due to a large error. After many times of fitting optimizations, the peak position and FWHM of core level curves are determined and their rationality is

analyzed by comparing the results reported in the literature. The fitting error is determined to be smaller than 10% in total.

XPS atomic ratios were determined according to the area ratio of the core lines (C_{1s}, O_{1s}, N_{1s} and Si_{2p}) and corrected for the corresponding theoretical atomic cross-sections and for a square root dependence of the photo-electrons kinetics energies. The element, Si, which may come from the impurities of raw graphite, was not under further consideration.

1.4 UV-Vis and Fluorescence spectra

UV-Vis spectra were recorded in quartz cuvettes (light path length 10 mm) on a Lambda 35 spectrometer (Perkin Elmer) in the range of 800 ~ 300 nm with a scan rate 240 nm/min and a resolution 1 nm. Fluorescence spectra were recorded in quartz cuvettes (light path length 10 mm) on an Edinburgh Instrument FLS 920 spectrophotometer. The fluorescence was monitored at 376 nm with the excitation 345 nm at room temperature (~19 °C) and the slit was kept constant for ensuring the comparability of all samples. The emission lifetime measurement (decay curve) was carried out using time-correlated single photon counting method (TCP) under the same condition. A peak counts of 1000 was selected and the time range is 200 ns. The instrument error was corrected using Ludox solution, prior to further analysis. For reference, the lifetimes before correction were 39.4 ns for 1-pyrenemethanol, 2.9 and 34.9 ns for HO-GNs, respectively. Data analysis was performed using the F900 data system. The decay curve of HO-GNs cannot be fitted when only one-exponential decay was adopted.

1.5 X-ray diffraction and Raman characterization

X-ray diffraction tests were carried out using a Rigaku D/max-γB X-ray diffractometer with Cu K_α radiation (λ = 1.54 Å) at a scanning rate of 3°/min in the ranging of 2θ=5~80°. Raman spectra were obtained using a multi-channel confocal microspectrometer (Dilor LABRAM-1B) with a laser wavelength 631 nm. Freshly prepared powder solids were used in both XRD and Raman.

1.6 Thermal study

Thermogravimetric analysis (TGA) was conducted with a TA Q5000 and nitrogen was used as the purge gas (25 ml/min). All samples were heated from ambient temperature to 700 °C at a 10 °C/min heating rate. Prior to testing, all samples were carefully grinded to powder, in order to ensure good heat conduction. Generally, 5 mg of sample was used for each test.

1.7 Dynamic mechanical analysis

Dynamic mechanical analysis (DMA) was performed on the DMA 242, from -90 to 100 °C with a frequency 1 Hz and a heating rate 3 °C/min in tensile configuration. PU and composite films were cut into strips (15×4×0.4 mm^3) prior to use. The samples were kept at -100 °C for at least 10 min to ensure that they were in the glass state.

1.8 Tensile tests

The mechanical properties of the neat PU and composite films were measured using a universal testing machine (CMT-4102, SANS Group, China) at room temperature with a tensile rate of 30 mm/min. All samples were cut into the dumbbell shape (20×4×0.4 mm^3) with a razor blade. Each sample repeated at least 5 times.

2. Dispersion of HO-GNs in different solvents

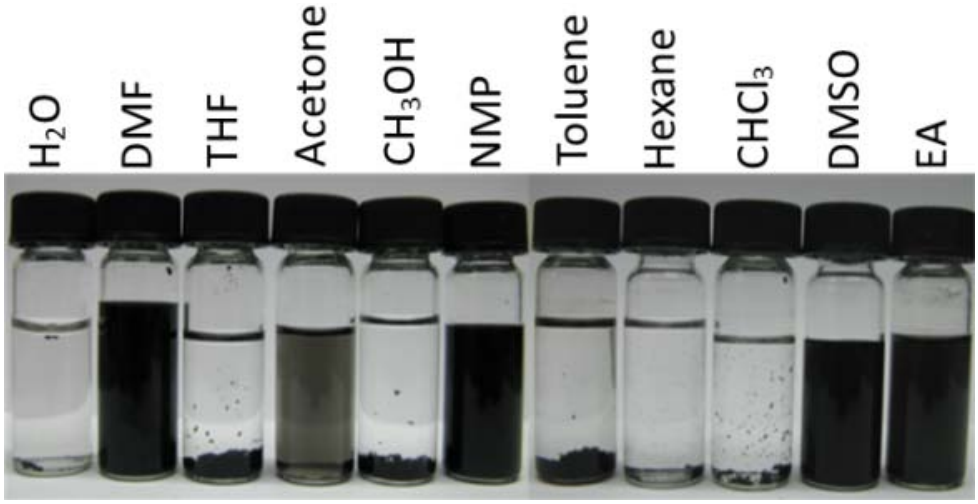

Figure S1 Dispersion status of HO-GNs in a variety of solvents including water, DMF, THF etc after 2 weeks.

PU oligomer chains decorated GNs (HO-GNs) facilitate the dispersion of hydrazine reduced GNs in organic solvents. We examined their dispersing capability in different solvents, including H_2O, DMF and THF etc. As shown in Figure S1, oligomer chains enable GNs to steadily disperse in DMF, NMP, DMSO and EA even after 2 weeks, but other solvents such as H_2O, THF etc exhibit relatively poor dispersing capability. This indicates the attached PU oligomer chains have transferred GNs into organophilic, which can improve their dispersion in the PU matrix.

3. XPS spectra of GO and HO-GNs

In Figure S2a,c,e, typical XPS spectra of GO, GNs and HO-GNs consist of two prominent bandgroups at 284 eV and 532 eV, corresponding to the C_{1s} and O_{1s} bands, respectively. Two additional weak bandgroups, N_{1s} bandgroup at 400 eV and Si_{2p} bandgroup at 104 eV, are also observed. The Si atoms may come from the impurities of graphite, which is not under further consideration. The C/O ratios of GO, GNs and HO-GNs are 2.26, 4.72 and 5.05, respectively, indicating a reduction in the number of oxygen functional groups of GNs and HO-GNs. The N atom percentage of GO is quite low (0.62%), with a C/N ratio of 103.8. It is supposed to arise from the sodium nitrate used in the oxidation or the impurities of nature graphite. The N atoms are not detected in the GNs, and thus also not further analyzed. The N atoms in HO-GNs (2.2%) primarily arise from the urethane groups and a higher C/N ratio (35.8) indicates that PU oligomer chains on the GN surface is less than the XPS probing depth (the effective sampling depth, z = 5.3 nm).

The high-resolution spectra of O_{1s} core-level in Figure S2 can be divided into two subpeaks, that is, a carboxyl peak located at 532.2 eV and a hydroxyl peak located at 533.4 eV.[3] The high-energy and low-energy tailings in HO-GNs reflect a combination of hole state lifetime broadening contributions from the urethane oxygen (N-COO) and ester (-COO-) groups.[3] The ratio of hydroxyl to carboxyl groups for GO and HO-GNs is higher to those calculated from C_{1s} core-level spectra, reflects the difference in the sampling depth. The similar case was also observed in Ref. 12. Because the O_{1s} photoelectron kinetic energies are lower than those of the C_{1s}, thus the O1s spectra should have a smaller sampling depth and be more surface specific. This result agrees well with the HO-GNs structure, where hydroxyl groups should be at the surface. The N_{1s} core-level spectra in Figure S2g,h, are not divided into subpeaks. According to

the literature,[4] the peak at 400.2 eV for HO-GNs is assigned to the -NH- (amine site) species. This peak is shifted to 400.6 eV in GO, reflects a higher content of N^+ (polaron site) species.

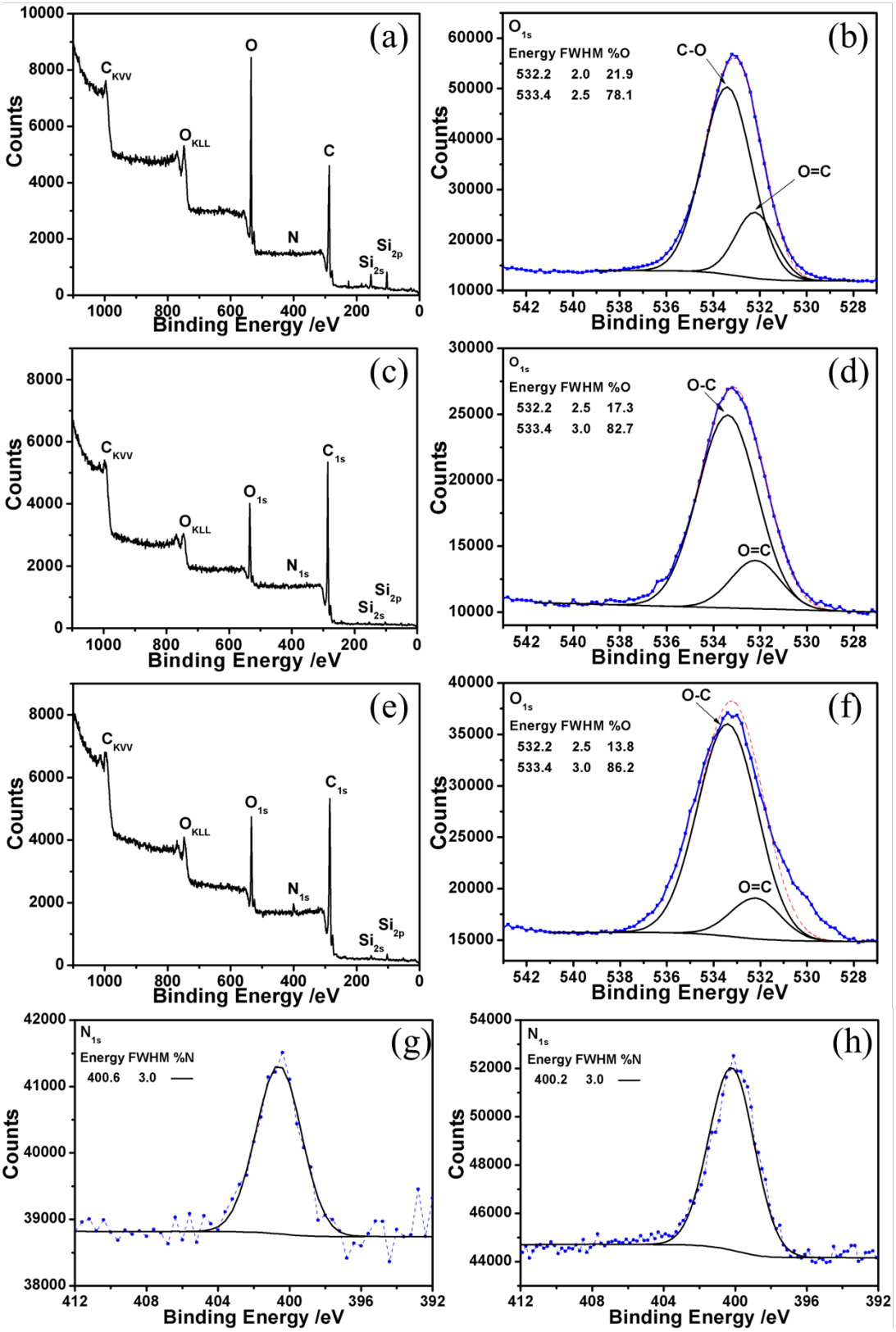

Figure S2 Wide scan XPS of (a) GO, (c) GNs and HO-GNs (e). Corresponding XPS core-level spectra: (b, d, f) O_{1s} of GO, GNs and HO-GNs; (g,h) N_{1s} of GO and HO-GNs, respectively.

4. Fluorescence study on the non-covalent bonding between pyrenemethanol and graphene

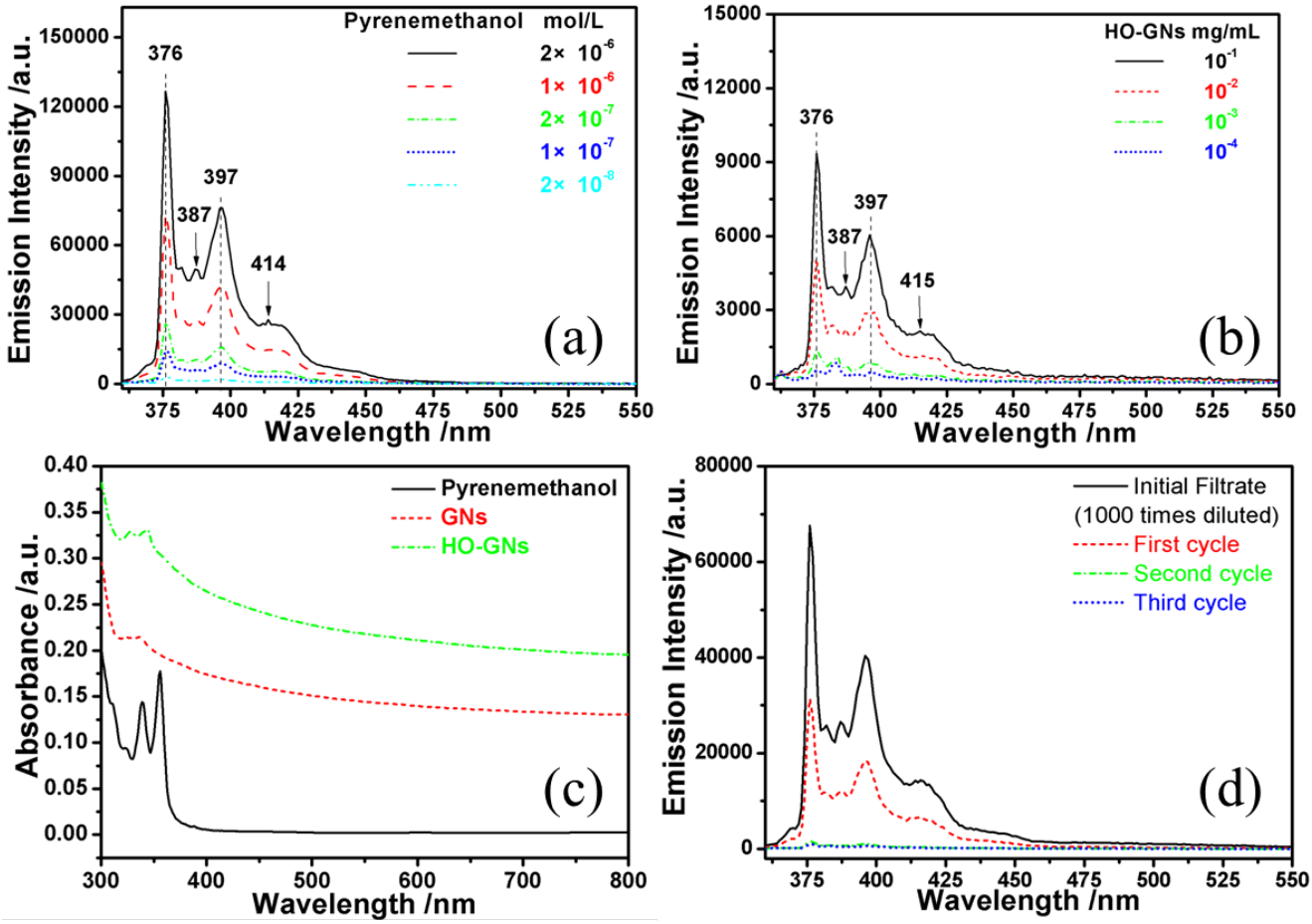

Figure S3 Fluorescence spectra (excited at 345 nm) of (a) 1-pyrenemethanol and (b) HO-GNs DMF solution at different concentration; (c) UV-Vis spectra of 1-pyrenemethanol (0.001 mg/ml), GNs (0.01 mg/ml) and HO-GNs (0.01 mg/ml) DMF solution. (d) Fluorescence spectra (excited at 345 nm) of the filtrate of the MDI-modified GNs with different DMF washing cycles.

We conducted UV-Vis and fluorescence experiments to investigate the interaction between pyrenemethanol and GNs. Pyrenemethanol has two characteristic peaks at 339 and 356 nm in the UV-Vis spectrum. These peaks are also observed in HO-GNs and blue-shifted to 328 and 344 nm, indicating the interaction between pyrenemethanol and GNs. It is difficult to investigate the effect of pyrenemethanol on the aromatic structure of GNs by UV-Vis spectra, as a result of the solvent effect (DMF). This interaction may be confirmed by the fluorescence data. As shown in Figure S3a, pyrenemethanol has four strong characteristic peaks at 376, 387, 397 and 415 nm, respectively. However, when it was attached to the GN surface, the fluorescence is significantly weakened and finally quenched at a low HO-GNs concentration due to the electronic or energy transfer. Note that the slit is kept constant for ensuring the comparability of all samples, and 1×10^{-6} mol/L pyrenemethanol corresponds to a mass concentration 2.32×10^{-4} mg/ml, a much lower concentration than that of HO-GNs. This indicates the strong interaction, *e.g.*, π-π interaction in the HO-GNs, and provides direct evidence for the non-covalent bonding between pyrenemethanol and GNs.

To confirm the removal of all the organics, the filtrate after MDI modification was collected and used for fluorescence studies. As shown in Figure S3d, no significant fluorescence of pyrenemethanol was observed after 2 cycles of DMF washing. The calculated pyrenemethanol concentration of initial filtrate is ~10^{-3} mol/L in terms of the data in Figure S3a, with a total amount of unreacted pyrenemethanol of 0.1 mmol (~10% of the feed amount). It is seen that despite the lost during washing and further reaction, most of pyrenemethanol molecules are adsorbed on GNs and finally converted into a short polyurethane chain, which is consistent with our TGA results.

5. XRD and Raman investigation on the structure of graphene

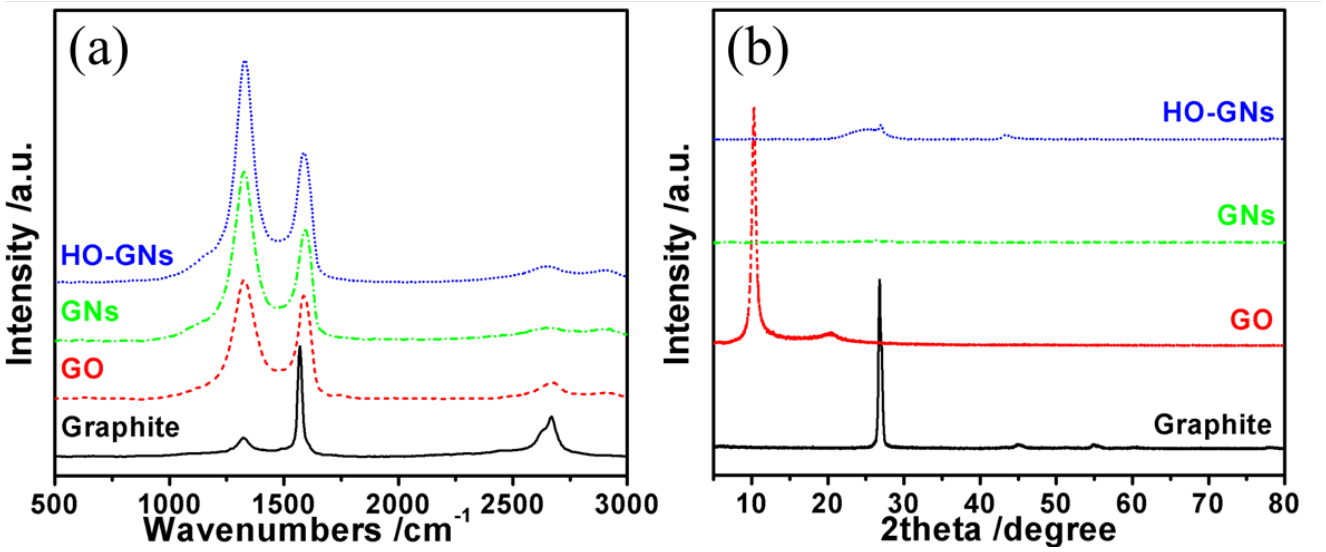

Figure S4 Raman (a) and XRD (b) spectra of GO, GNs, HO-GNs and graphite.

Raman spectra reflect the integrity of GNs by measuring the two primary characteristic bands: 1580 cm^{-1} (G band) and 1325 cm^{-1} (D band).[5] The former corresponds to the sp^2 carbon atom from the aromatic structure in GNs while the latter represents the contribution from sp^3 carbon atoms of defect structures. For the as-received graphite sample, as shown in Figure S4a, the G band is the primary characteristic band and the small D band would originate from the contribution of the edge sp^3 carbon atoms. After oxidization, a remarkable enhancement in intensity of the D band is observed and no obvious intensity changes appeared even after reduction with hydrazine and decoration with pyrene derivatives with oligomer short chains. This is consistent with the results observed in other reports. It was concluded that hydrazine reduction is not very sensitive to the D band variation. To quantify the effect of oxidization and reduction on the crystal structure of GNs, a Raman technique has been proposed to characterize the size of crystal domains in GNs (L_a), that is, $L_a(\mathrm{nm}) = 2.4 \times 10^{-10} \times \lambda_{laser}^4 \times (I_D/I_G)^{-1}$.[6] In terms of this method, graphite, the determined crystal domain sizes of GO, GNs and HO-GNs are 223.8, 33.0, 24.9 and 22.2 nm, respectively. Apparently, the destruction of oxidization reaction to the crystal structure of GNs is significant, but the contribution of hydrazine reduction to recovery of the crystal structure is limited. An interesting phenomenon is that the crystal sizes of GNs and HO-GNs continue to decrease compared to that of GO, which could stem from the decreased graphene size and more sp^3 carbon atoms located at the edge.

Figure S4b shows the XRD patterns of graphite, GO, GNs and HO-GNs. The as-received graphite exhibits a characteristic diffraction peak at 26.8°, corresponding to an interlayer spacing of 0.33 nm in terms of Bragg equation ($2d\sin\theta = k\lambda, \lambda = 0.154$ nm). The strong diffraction peak of GO at 10.3° indicates an interlayer spacing of 0.86 nm. The increased interlayer spacing primarily originates from the presence of a large amount of oxygen functional groups. Interestingly, for GNs and HO-GNs, the former do not reveal any diffraction peak in the detected angle range while the latter shows a weak, broad diffraction peak around 24.0° and another smaller peak at 26.9°, corresponding to interlayer distances of 0.37 and 0.33 nm, respectively. The good exfoliation state of GNs (no diffraction peak) is probably related to the loss of oxygen functional groups in the basal plane of GNs, which impairs the H-bond interaction between GNs so that they stack together in a relatively loose manner. In addition, the reduction in the sheet size is probably the other reason to form loose stacking. Two weak diffraction peaks observed in HO-GNs presumably stem from the tight stacking between pyrene rings and GNs. The stronger diffraction at 24.0° than that at 26.9° suggests that the majority of the pyrene rings could be adsorbed on the GN surface in a loose manner due to the presence of a significant amount of defects in the GN crystal plane. It is also supported by decay curves of HO-GNs, that two life-time (1.2 and 33.2 ns) are observed. The latter may originate from the adsorbed pyrenemethanol molecules that stack with each other in a loose manner.

6. SEM fractographs of cryogenically fractured the neat PU and GN/PU elastomer films

Figure S5 shows the SEM images of cryogenically fractured neat PU and composite elastomer films with different HO-GN contents. The neat PU reveals ordered ripple structures in its fractograph, which means that the propagation of cracks is less limited in this cryogenically treated PU sample. However, the ripple structures are suppressed in the composites and the fractured surface becomes rougher with increasing HO-GN contents. Further observation for Figure S5b-d shows that these HO-GNs are not well extended but dispersed in the PU matrix in a bended or distorted conformation, which is similar to the SEM observation by Choi *et al.*[7] This distorted morphology is related to the inherent flexibility of GNs. On the whole, the dispersion of HO-GNs in the PU is uniform except that a few aggregates are observed in these composites, which have also been observed in other graphene-based composites and suggested presumably arising from the interaction between GNs and the matix, as well as the preparation process of samples.

Figure S6 shows the amplified SEM images of the neat PU and composite films. The samples for SEM observation are fractured after dipping in liquid nitrogen for 30 min. The fractograph of the neat PU film shows relatively regular crack propagation, as marked by red arrows in Figure S6a, and the fracture surface is smooth, as marked by green arrows. In contrast, the composite film reveal rougher fracture surface (green arrows) in which the crack becomes distorted, as denoted by red arrows in Figure S6b,c,d. The rough morphology for these composite films means that the added HO-GNs inhibited the propagation of cracks to some extent, which is consistent with the case of GN/epoxy composites.[8-10] It would note that such a cryogenic fractograph is different from the case that they are fractured at room temperature or above the glass transition temperature of the matrix, as mentioned in the Introduction. Nevertheless, such an observation for the brittle fracture behavior is helpful for evaluating whether HO-GNs are uniformly dispersed in the matrix.

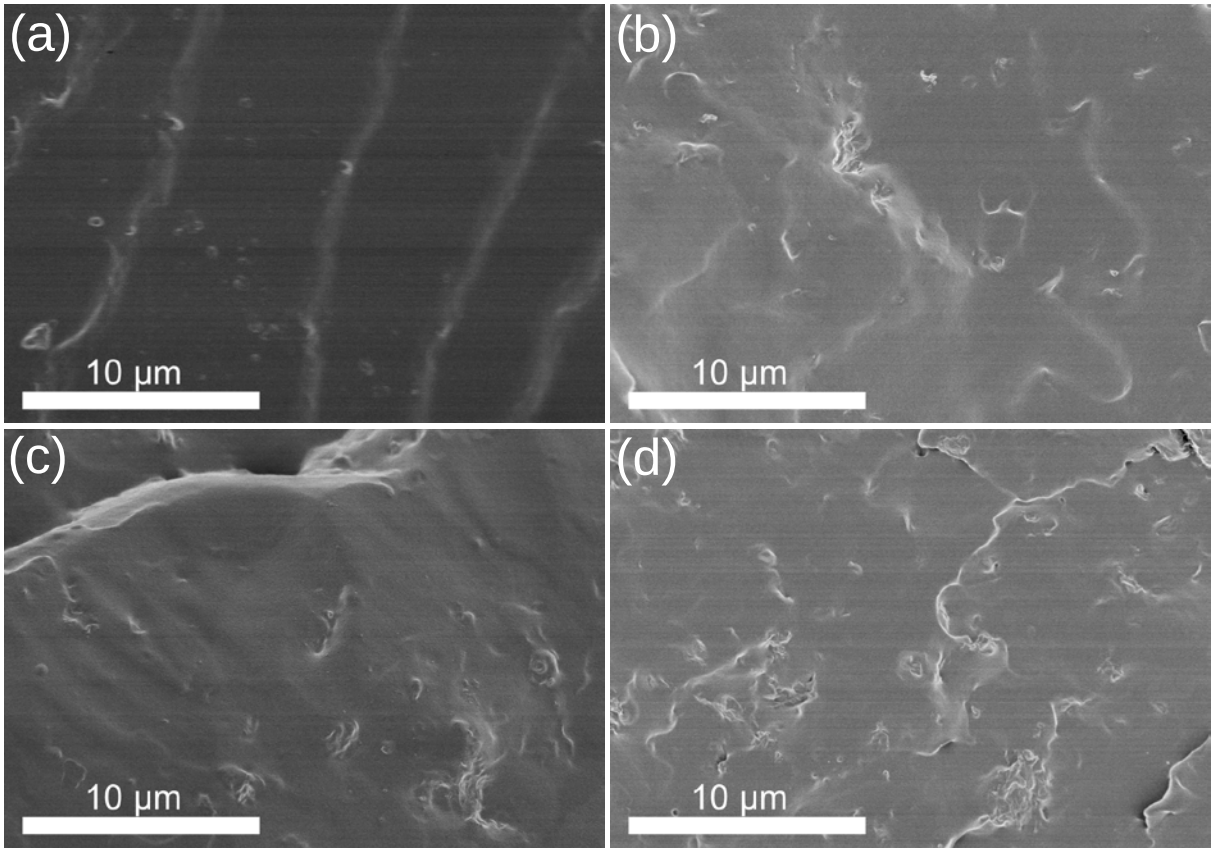

Figure S5 SEM fractographs of (a) the neat PU, composites with (b) 0.5 wt%, (c) 1.0 wt% and (d) 2.0 wt% HO-GNs.

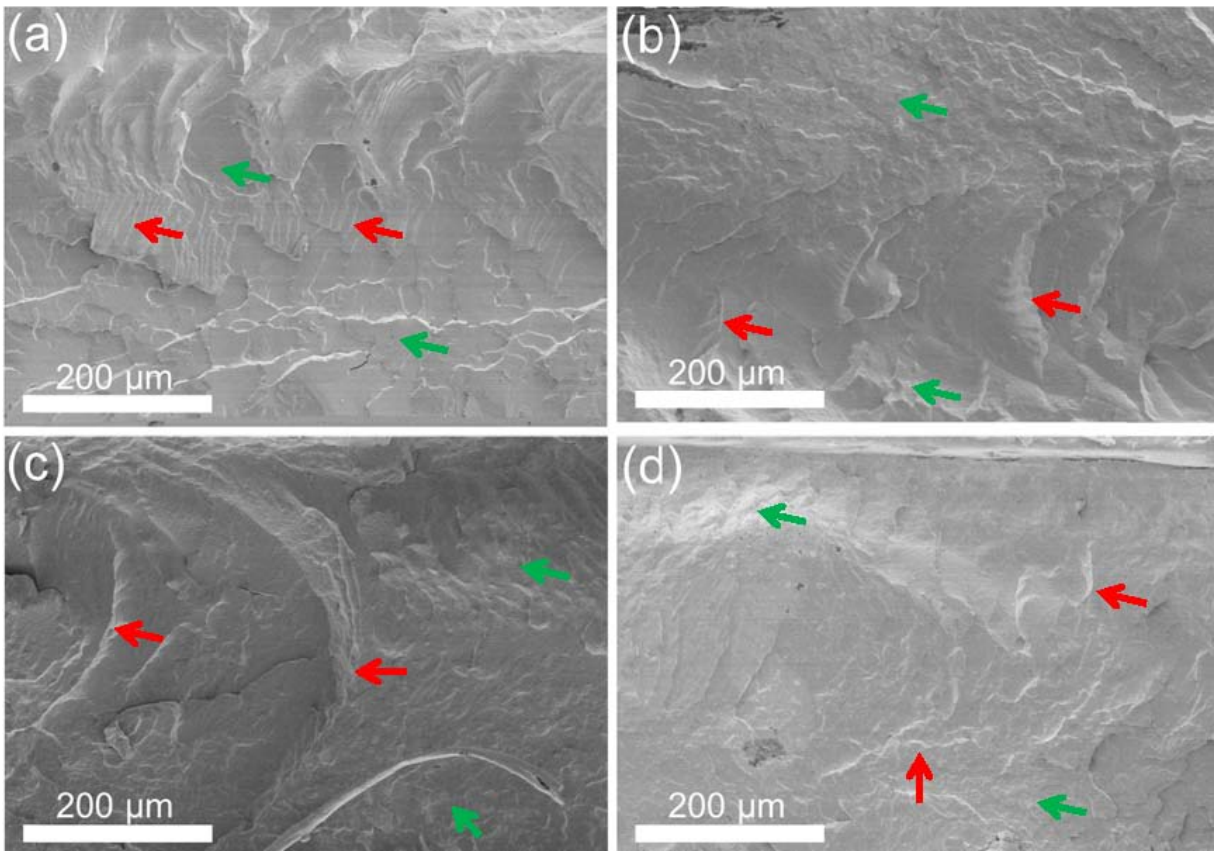

Figure S6 Amplified SEM fractographs of the neat PU and composite elastomer films (the HO-GN content in each image is the same as that in Figure S5).

7. Dynamic mechanical analysis of the neat PU and composite elastomer films

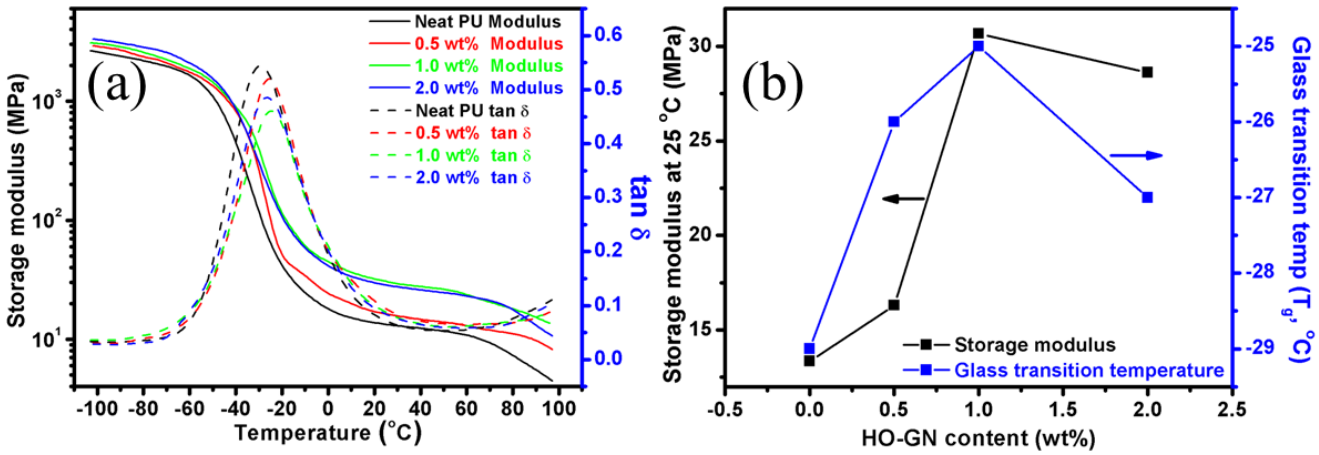

Figure S7 Dynamic mechanical analysis results of the neat PU and composite elastomer films. (a) Storage modulus and *tan θ* versus temperature: solid—storage modulus, dash--*tan θ* changes of storage modulus at 40 °C and glass transition temperatures with HO-GNs contents.

Figure S7a shows the dynamic modulus and *tan θ* curves of the neat PU and composite films, from which the glass transition temperature (T_g) and storage modulus at 25 °C are extracted and the results are showed in Figure S7b. The storage modulus at 25 °C for the neat PU film is 13.35 MPa while for the 1.0 wt% composite film the value increases to 30.68 MPa, increasing by 129.8%. This is comparable to the observation in static tensile measurements. Similarly, the 2.0 wt% composite film also reveals a decrease in storage modulus relative to the 1.0 wt% sample. This can be attributed to the introduction of more free volume in the composite with high HO-GNs content, as described in the context and our previous study.[11] Such an increase in free volume is also in agreement with the change of T_gs, for which an abnormal decrease for the 2.0 wt% sample is observed.

References

1. Kvande, I.; Zhu, J.; Zhao, T.J.; Hammer, N.; Rønning, M.; Raaen, S.; Walmsley, J.C.; Chen, D. Importance of Oxygen-Free Edge and Defect Sites for the Immobilization of Colloidal Pt Oxide Particles with Implications for the Preparation of CNF-Supported Catalysts. *J. Phys. Chem.* C, **2010**, 114, 1752-1762.
2. Stankovich, S.; Dikin, D.A.; Piner, R.D.; Kohlhass, K.A.; Kleinhammes, A.; Jia, Y.Y.; Wu, Yue; Nguyen, S.B.T; Ruoff, R.S. Synthesis of Graphene-Based Nanosheets via Chemical Reduction of Exfoliated Graphite Oxide. *Carbon*, **2007**, 45, 1558-1565.
3. Korematsu, A.; Takemoto, Y.; Nakaya, T.; Inoue, H. Synthesis, Characterization and Platelet Adhesion of Segmented Polyurethanes Grafted Phospholipid Analogous Vinyl Monomer on Surface. *Biomaterials*, **2002**, 23, 263-271.
4. Wen, T.C.; Wu, M.S.; Yang, C.H. Spectroscopic Investigations of Poly(oxypropylene)glycol-Based Waterborne Polyurethane Doped with Lithium Perchlorate. *Macromolecules*, **1999**, 32, 2712-2720.
5. Pimenta, M.A.; Dresselhaus, G.; Dresselhaus, M.S.; Cancado, L.G.; Jorio, A.; Saito R. Studying Disorder in Graphene-Based Systems by Raman Spectroscopy. *Phys. Chem. Chem. Phys.* **2007**, 9, 1276-1291.

6. Cancado, L.; Takai, K.; Enoki, T.; Endo, M.; Kim, Y.A.; Mizusaki, H.; Jorio, A.; Coelho, L.N.; Magalhaes-Paniago, R.; Pimenta, M.A. General Equation for the Determination of the Crystallite Size L-a of Nanographite by Raman Spectroscopy. *Appl. Phys. Lett.* **2006**, 88, 163106.
7. Choi, J. T.; Kim, D. H.; Ryu, K. S.; Lee, H. I.; Jeong, H. M.; Shin, C. M.; Kim, J. H.; Kim, B. K. Functionalized Graphene Sheet/Polyurethane Nanocomposites: Effect of Particle Size on Physical Properties. *Macromol. Res.* **2011**, 19, 809-814.
8. Rafiee, M. A.; Rafiee, J.; Wang, Z.; Song, H. H.; Yu, Z. Z.; Koratkar, N. Enhanced Mechanical Properties of Nanocomposites at Low Graphene Content. *ACS Nano* **2009**, 3, 3884-3890.
9. Rafiee, M. A.; Rafiee, J.; Srivastava, I.; Wang, Z.; Song, H. H.; Yu, Z. Z.; Koratkar, N. Fracture and Fatigue in Graphene Nanocomposites. *Small* **2010**, 6, 179-183.
10. Yavari, F.; Rafiee, M. A.; Rafiee, J.; Yu, Z. Z.; Koratkar, N. Dramatic Increase in Fatigue Life in Hierarchical Graphene Composites. *ACS Appl. Mater. Interfaces* **2010**, 2, 2738-2743.
11. Pan, Y. Z.; An, L.; Xu, Y.; Lu, H. B.; Yang, Y. L.; Chen W.; Nutt, S. Hybrid Network Structure and Mechanical Properties of Rodlike Silicate/Cyanate Ester Nanocomposites. *Macromolecules* **2008**, 41(23), 9245-9258.
12. Yang. D.X.; Velamakanni A.; Bozoklu, G.; Park, S.J.; Stoller, M.; Piner, R.D.; Stankovich, S.; Jung, I.; Field, D.A.; Ventrice, C.A.; Ruoff, R.S. Chemical Analysis of Graphene Oxide Films after Heat and Chemical Treatments by X-ray Photoelectron and Micro-Raman Spectroscopy. *Carbon* **2009**, 47, 145-152.